

Supporting information

Polarizability is a Key Parameter for Molecular Electronics

Angélique Gillet,^a Sébastien Cher,^a Marine Tassé,^b Thomas Blon,^a Sandra Alves,^c Guillaume Izzet,^c
Bruno Chaudret,^a Anna Proust,^c Phillippe Demont,^d Florence Volatron,^{c,*} and Simon Tricard^{a,*}

^a *Laboratoire de Physique et Chimie des Nano-Objets, INSA, CNRS, Université de Toulouse, Toulouse, France*

^b *Laboratoire de Chimie de Coordination, CNRS, Université de Toulouse, Toulouse, France*

^c *Institut Parisien de Chimie Moléculaire, CNRS, Sorbonne Université, Paris, France*

^d *Institut Carnot – Centre Inter-universitaire de Recherche et d'Ingénierie des Matériaux, INP-ENSIACET, CNRS, Université de Toulouse, Toulouse, France*

* *Corresponding authors: florence.volatron@sorbonne-universite.fr, tricard@insa-toulouse.fr*

Table of content:

Experimental section.....	2
Supplementary characterization data.....	10

Experimental section

Chemical Syntheses

Polyoxometalates.

All chemicals and solvents were purchased from Aldrich, VWR and Alfa Aesar and used as received.

$(\text{TBA})_3[\alpha\text{-PW}_{12}\text{O}_{40}]$, $\text{K}_7[\alpha\text{-PW}_{11}\text{O}_{39}]\cdot 14\text{H}_2\text{O}$, $\text{K}_8[\alpha\text{-SiW}_{11}\text{O}_{39}]\cdot 13\text{H}_2\text{O}$ and $\text{K}_9[\alpha\text{-AlW}_{11}\text{O}_{39}]\cdot 13\text{H}_2\text{O}$ were prepared following published procedures (TBA stands for tetrabutylammonium cations):

- $(\text{TBA})_3[\alpha\text{-PW}_{12}\text{O}_{40}]$: C. Rocchiccioli-Deltcheff et al., *Inorg. Chem.* **1983**, 22, 207,
- $\text{K}_7[\alpha\text{-PW}_{11}\text{O}_{39}]\cdot 14\text{H}_2\text{O}$: P. Souchay in *Polyanions et polycations*, Gauthier-Villars, Paris, **1963**,
- $\text{K}_8[\alpha\text{-SiW}_{11}\text{O}_{39}]\cdot 13\text{H}_2\text{O}$: A. Tézé et al. *Inorg. Synth.*, **1990**, 27, 85,
- and $\text{K}_9[\alpha\text{-AlW}_{11}\text{O}_{39}]\cdot 13\text{H}_2\text{O}$: J.J. Cowan et al., *Inorg. Synth.*, **2002**, 33, 18.

$(\text{TBA})_3[\text{PW}_{11}\text{O}_{39}\{\text{O}(\text{SiC}_3\text{H}_6\text{SH})_2\}]$ (**POM-P**). The synthesis of **POM-P** has been already detailed elsewhere [B. Martinez et al., *J. Phys. Chem. C*, **2018**, 122, 26680]. Briefly, POM-P was formed by the condensation of the $(\text{OCH}_3)_3\text{SiC}_3\text{H}_6\text{SH}$ silane on the $\text{K}_7 \alpha\text{-PW}_{11}\text{O}_{39}\cdot 14\text{H}_2\text{O}$ precursor in a mixed water/acetonitrile medium at acidic pH and low temperature. The compound was recovered by adding an excess of tetrabutylammonium bromide (TBABr), and washed with diethylether to give a white powder with a good yield (76%).

^1H NMR (400 MHz, CD_3CN) : δ (ppm) 3.12 (m, 24H), 2.64 (m, 4H), 1.87 (m, 4H), 1.63 (m, 24H), 1.39 (sex, $^3\text{J}(\text{H,H})=7.4\text{Hz}$, 24H), 0.99 (t, $^3\text{J}(\text{H,H})=7.4\text{Hz}$, 36H), 0.90 (m, 4H) ; ^{31}P NMR (162 MHz, CD_3CN) δ (ppm) -12.37 ; IR (KBr pellet) : $\nu=2962$ (m), 2934 (m), 2873 (w), 2567 (vw, SH), 1483 (m), 1381 (w), 1111 (s, PO), 1065 (s, PO), 1052 (s, SiO), 1036 (s, SiO), 963 (vs), 870 (vs), 824 (vs), 711 (m), 585 (w), 522 (m), 383 cm^{-1} (s) ; HRMS (ESI-), m/z (%) calcd for $\text{C}_6\text{H}_{14}\text{O}_{40}\text{PS}_2\text{Si}_2\text{W}_{11}$: 966.75 $[\text{M}]^{3-}$; found : 966.75 ; calcd for $\text{C}_{22}\text{H}_{50}\text{NO}_{40}\text{PS}_2\text{Si}_2\text{W}_{11}$: 1571.26 $[\text{M} + \text{TBA}]^{2-}$; found : 1571.26; Elemental Analysis calcd (%) for $\text{C}_{54}\text{H}_{122}\text{N}_3\text{O}_{40}\text{PS}_2\text{Si}_2\text{W}_{11}$: C 17.87, H 3.36, N 1.16; found : C 17.98, H 3.22, N 0.92

(TBA)₄[SiW₁₁O₃₉{O(SiC₃H₆SH)₂}] (POM-Si). K₈ α-SiW₁₁O₃₉.13H₂O (0,4 g, 0.124 mmol) was dissolved in 20 mL of water. 15 mL of acetonitrile were added. Then 0.4 mL of diluted HCl (1M in water) was added to the turbid solution that became almost clear and reached a pH around 4. The mixture was cooled in an ice bath before the slow addition of the (OCH₃)₃SiC₃H₆SH silane (0.097 mL, 0.497 mmol). Then 1 mL of diluted HCl was added to reach an apparent pH of 2 and the solution was kept under stirring during one night. Then TBABr (0,16 g, 0.497 mmol) was added to the clear solution and lead to the formation of a white precipitate. The powder was recovered by centrifugation, dissolved in 15 mL of acetonitrile then precipitated again thanks to the addition of an excess (10 éq) of TBABr and absolute ethanol. The white powder, recovered by centrifugation was washed with absolute ethanol and ether then dried under vacuum (yield 77%).

¹H NMR (400 MHz, CD₃CN) : δ (ppm) 3.15 (m, 32H), 2.64 (m, 4H), 1.86 (m, 4H), 1.64 (m, 32H), 1.40 (sex, ³J(H,H)=7.4Hz, 32H), 0.99 (t, ³J(H,H)=7.4Hz, 48H), 0.76 (m, 4H) ; ²⁹Si NMR (119 MHz, DMSO-d₆) δ (ppm) -53.07 (O-Si-C₃H₆-SH), -85.11 (Si-O-W) ; IR (KBr pellet) : ν=2961 (m), 2935 (m), 2874 (w), 2567 (vw, SH), 1484 (m), 1381 (w), 1043 (s, SiO), 1018 (s, SiO), 963 (s), 947 (s), 904 (vs), 855 (s), 806 (vs), 754 (sh), 710 (sh) 535 (m), 389 cm⁻¹ (s) ; HRMS (ESI-), m/z (%) calcd for C₆H₁₄O₄₀S₂Si₃W₁₁ : 724.31 [M]⁴⁺ ; found : 724.31 ; calcd for C₂₂H₅₀NO₄₀S₂Si₃W₁₁ : 1046.51 [M + TBA]³⁻ ; found : 1046.51 ; calcd for C₃₈H₈₆N₂O₄₀S₂Si₃W₁₁ : 1690.90 [M + 2TBA]²⁻ ; found : 1690.91 ; Elemental Analysis calcd (%) for C₇₀H₁₅₈N₄O₄₀S₂Si₃W₁₁ : C 21.74, H 4.09, N 1.45; found : C 21.70, H 3.97, N 1.43.

(TBA)₅[AlW₁₁O₃₉{O(SiC₃H₆SH)₂}] (POM-Al). K₉ α-AlW₁₁O₃₉.13H₂O (0,4 g, 0.123 mmol) was dissolved in a mixture of water (20 mL) and acetonitrile (15 mL). Then 0.35 mL of diluted HCl (1M in water) was added. The turbid solution at pH=4 was cooled in an ice bath before the slow addition of the (OCH₃)₃SiC₃H₆SH silane (0.093 mL, 0.49 mmol). 0.6 mL of 1M HCl was then added to reach a pH around 2 and make the solution clear, which was kept one night under stirring. Then TBABr (792 mg, 2,46 mmol) was added to the solution and an abundant white precipitate formed. After centrifugation the solid was dissolved in the minimum of acetonitrile then precipitated again with an

excess of absolute ethanol. The white powder was washed with absolute ethanol and ether then dispersed in dichloromethane, in which 400 mg of TBABr and 0.5 mL of triethylamine were added. The insoluble was separated by centrifugation and the filtrate concentrated in the rotary evaporator until the appearance of the first solid particles then an excess of absolute ethanol was added to make precipitate the product. The white powder was washed with absolute ethanol and ether and dried under vacuum (yield 75 %).

^1H NMR (400 MHz, CD_3CN) : δ (ppm) 3.18 (m, 40H), 2.62 (m, 4H), 1.84 (m, 4H), 1.65 (m, 40H), 1.41 (sex, $^3\text{J}(\text{H,H})=7.4\text{Hz}$, 40H), 0.98 (t, $^3\text{J}(\text{H,H})=7.4\text{Hz}$, 60H), 0.64 (m, 4H) ; ^{27}Al NMR (104 MHz, CD_3CN) δ (ppm) 72.1 ; IR (KBr pellet) : $\nu=2960$ (m), 2934 (m), 2872 (w), 2551 (vw, SH), 1484 (m), 1381 (w), 1035 (s, SiO), 1009 (s, SiO), 943 (vs), 928 (s), 881 (vs), 852 (s), 803 (vs), 546 (m), 473 (m), 384 cm^{-1} (s) ; HRMS (ESI-), m/z (%) calcd for $\text{C}_{38}\text{H}_{86}\text{N}_2\text{O}_{40}\text{AlS}_2\text{Si}_2\text{W}_{11}$: 1126.94 [M + 2TBA] $^{3-}$; found : 1126.94 ; calcd for $\text{C}_{54}\text{H}_{122}\text{N}_3\text{O}_{40}\text{AlS}_2\text{Si}_2\text{W}_{11}$: 1811.55 [M + 3TBA] $^{2-}$; found : 1811.55 Elemental Analysis calcd (%) for $\text{C}_{86}\text{H}_{194}\text{N}_5\text{O}_{40}\text{AlS}_2\text{Si}_2\text{W}_{11}$: C 25.14, H 4.72, N 1.70 ; found : C 24.87, H 4.59, N 1.49.

(TBA_{4.1}H_{0.9})[AlW₁₁O₃₉{O(SiC₃H₆SH)₂}] (POM-AIH). The synthesis of **POM-AIH** followed exactly the procedure used for the synthesis of the **POM-AI** (see above) until the stirring of the solution during one night. Then, TBABr (198 mg, 0.615 mmol) was added to the clear solution and a white precipitate formed. The solid was recovered by centrifugation, dissolved in the minimum of acetonitrile then precipitated with an excess of ether, washed with ether and dried under vacuum (yield 76%).

^1H NMR (400 MHz, CD_3CN) : δ (ppm) 3.14 (m, 33H), 2.62 (m, 4H), 1.82 (m, 4H), 1.64 (m, 33H), 1.40 (sex, $^3\text{J}(\text{H,H})=7.4\text{Hz}$, 33H), 0.98 (t, $^3\text{J}(\text{H,H})=7.4\text{Hz}$, 49H), 0.74 (m, 4H) ; ^{27}Al NMR (104 MHz, CD_3CN) δ (ppm) 71.7 ; IR (KBr pellet) : $\nu=2961$ (m), 2935 (m), 2874 (w), 2564 (vw, SH), 1484 (m), 1381 (w), 1034 (s, SiO), 1009 (s, SiO), 955 (vs), 937 (s), 888 (vs), 859 (s), 795 (vs), 541 (m), 470 (m), 383 cm^{-1} (s) ; Elemental Analysis calcd (%) for $\text{C}_{86}\text{H}_{194}\text{N}_5\text{O}_{40}\text{AlS}_2\text{Si}_2\text{W}_{11}$: C 22.10, H 4.18, N 1.48 ; found : C 22.22, H 3.80, N 1.53.

Platinum nanoparticles. The PtNPs have been synthesized as followed (S. Gomez et al., *Chem. Commun.* **2001**, 1474 ; S. Tricard et al., *Mater Horiz* **2017**, *4*, 487). All operations were carried out using Fischer-Porter bottle techniques under argon. A solution of Pt₂(dba)₃ (90 mg; 0.165 mmol of Pt) in 20 mL of freshly distilled and deoxygenated THF was pressurized in a Fischer-Porter bottle with 1 bar of CO during 30 minutes at room temperature under vigorous stirring. During this time, the solution color changed from violet to brown (attesting the formation of the NPs). The mixture was evaporated and washed with pentane to eliminate the dba (3 x 20 mL), and to obtain native NPs. The colloid was then redissolved in 20 mL of acetonitrile. The size of the NPs was found to be between 1.7 ± 0.3 nm and 2.1 ± 0.4 nm.

Self-assembly. 1 mL of a solution of **POM** (at 6.10^{-3} mol.L⁻¹ in acetonitrile) was added to 4 mL of the native NP mixture under vigorous mixing. The precursor concentrations were adapted to obtain 0.2 eq. of **POM** per introduced Pt. The brown solution was agitated for 2 hours. Drops of the crude solution were deposited on specific substrates for each characterization (see below). The remaining solution was evaporated to dryness and was isolated as dark-brown powder. For each series of measurements, the sizes were determined by TEM imaging.

Characterization of the polyoxometalates

NMR spectroscopy. ¹H and ³¹P spectra were recorded on a Bruker AvanceIII Nanobay 400 MHz spectrometer, the ²⁷Al spectrum on a Bruker AvanceI 400 MHz and the ²⁹Si spectrum on a Bruker Avance III 600 MHz, all equipped with a BBFO probehead. ¹H and ²⁹Si chemical shifts are quoted as parts per million (ppm) relative to tetramethylsilane using the solvent signals as secondary standard (s: singlet, d: doublet, t: triplet, sex: sextet, m: multiplet) and coupling constants (J) are quoted in Hertz (Hz). ³¹P and ²⁷Al and ²⁹Si chemical shifts are quoted relative to 85% H₃PO₄ and Al(NO₃)₃ 1M in D₂O, respectively. All spectra were recorded in CD₃CN, except for the POM-Si, poorly soluble in acetonitrile, which was dissolved in DMSO-d₆ to record the ²⁹Si spectrum.

IR spectroscopy. IR spectra of all the powders were recorded from a KBr pellet on a Jasco FT/IR 4100 spectrometer (32 scans, resolution 4 cm⁻¹).

Mass spectrometry. High-resolution ESI mass spectra were recorded using an LTQ Orbitrap hybrid mass spectrometer (ThermoFisher Scientific, Bremen, Germany) equipped with an external ESI source operated in the negative ion mode. Spray conditions included a spray voltage of 3.5 kV, a capillary temperature maintained at 270 °C, a capillary voltage of -40 V, and a tube lens offset of -100 V. Sample solutions in acetonitrile (10 pmol.μL⁻¹) were infused into the ESI source by using a syringe pump at a flow rate of 180 μL.h⁻¹. Mass spectra were acquired in the Orbitrap analyzer with a theoretical mass resolving power (R_p) of 100 000 at m/z 400, after ion accumulation to a target value of 10⁵ and a m/z range detection from m/z 300 to 2000. All data were acquired using external calibration with a mixture of caffeine, MRFA peptide and Ultramark 1600 dissolved in Milli-Q water/ HPLC grade acetonitrile (50/50, v/v).

Elemental analysis. Elemental analyses were performed at the Institut de Chimie des Substances Naturelles, Gif sur Yvette, France, for the **POM-P**, **POM-Si** and **POM-AI** and at the Laboratoire de Chimie de Coordination, Toulouse, France for the **POM-AIH**.

Electrochemistry. Electrochemical studies were performed on an Autolab PGSTAT 100 workstation (Metrohm) using a standard three-electrode set-up. Glassy carbon electrode, platinum wire and saturated calomel electrode (SCE) were used as the working, auxiliary and reference electrode, respectively. The cyclic voltammograms were recorded in 1 mM solutions of the POMs in acetonitrile with tetrabutylammonium hexafluorophosphate TBAPF₆ as electrolyte (0.1 M), at a scan rate of 0.1 V.s⁻¹. To get around the problem of solubility of POM-Si, the POM was dissolved first in a drop of DMF then an excess of acetonitrile was added to fill the electrochemical cell.

Detailed interpretation of the POM characterization. On the NMR spectra, the typical peaks of the TBA counter cations were present, as well as three supplementary multiplets, integrating for four protons and corresponding to the methylene groups of the aliphatic arms wearing the thiol group (Fig. S1 to S3). The comparison of the three ^1H NMR spectra (Fig. S4) showed, as expected, an increasing of the TBA/methylene peaks ratio, as the POM charge increased. In addition, the multiplet corresponding to the closest methylene from the POM inorganic core shifted significantly from **POM-P** ($\delta= 0.90$ ppm), to **POM-Si** ($\delta= 0.76$ ppm) to **POM-Al** ($\delta= 0.64$ ppm), probably due to the charge variation, which modulates the number of counter cations surrounding the POM. IR spectroscopy confirmed the structural features of the three POMs (Fig. S5): the main bands of the TBA counter cations (around 2900, at 1484 and at 1381 cm^{-1}) and of the POMs inorganic core (between 300 and 1150 cm^{-1}) were observed on all the spectra, as well as the vibration bands of the S-H and the Si-O bonds, characteristic of the organic arm of the hybrid POMs. Mass spectrometry was in agreement with the proposed chemical structures of the three POMs (Fig. S6 to S8). Elemental analysis confirmed the number of TBA surrounding the POMs and thus their charges: 3- for **POM-P**, 4- for **POM-Si** and 5- for **POM-Al**.

Structural characterization of nanoparticles and self-assemblies

Transmission Electron Microscopy. Samples for TEM were prepared by deposition of one drop of the crude solution on a carbon covered holey copper grid. TEM analyses were performed at the “centre de microcaractérisation Raimond Castaing” using a JEOL JEM 1400 electron microscope operating at 120 kV. The mean size of the particles was determined by image analysis on a large number of particles (~300) using the ImageJ software.

Infrared spectroscopy. FT-IR spectra were recorded on a Thermo Scientific Nicolet 6700 FT-IR spectrometer in the range 4000-700 cm^{-1} , using a Smart Orbit ATR platform. The sample deposition was performed by drop casting of the crude solution on the germanium crystal of the platform; the measurement was acquired after evaporation of the acetonitrile solvent.

Small angle X-ray scattering. SAXS patterns were recorded on a PANalytical Empyrean diffractometer using the Co K α radiation. Small angle measurements were performed on a microscopy glass, on which the crude solution was drop casted. An advantage of working with particles smaller than 2 nm is that the inter-particle distance is sufficiently small to observe correlation distances between two particles with a regular XRD diffractometer without the need of any dedicated SAXS facilities.

Charge transport measurement

Dielectric constant. Dielectric spectroscopy measurements were performed on powder samples compacted between two stainless steel electrodes (diameter 10 mm) in a Teflon sample holder. The thickness of the powder was as small as possible (~400 μ m) to increase the sensitivity of the measurement. Dielectric measurements were carried out as a function of frequency (10^{-2} - 10^6 Hz) and temperature (100 -296 K) using a Novocontrol broadband dielectric spectrometer at an applied AC of 1 V_{rms}. Frequency sweeps were carried out isothermally. The intrinsic dielectric constant of the free aryl ligands was obtained from the real part $\epsilon'(\omega)$ of the complex dielectric permittivity $\epsilon^*(\omega)$ taken at a high frequency of 1MHz.

I-V curve measurement. Conductive AFM measurements were performed with an AIST-NT SmartSPM 1000 microscope, equipped with a conductive AFM unit. The samples were prepared by drop casting of one drop of the crude solution on silicon wafers covered by a ~50 nm layer of gold (with a ~5 nm chromium anchoring layer). We used conductive silicon tips covered by platinum (Mikromash HQ-NSC15/Pt). Typical measurements consisted in first performing a topography image of the sample and then going in contact on zones with individual assemblies to measure their I-V characteristics. Measurements were performed on several objects per zone and several zones of the substrates.

Data analysis. The I - V characteristics were normalized at 2 V. We then averaged the characteristics on 50 curves (error bars on the graphs are 95% confidence intervals). In order to fit the $I \propto V^\xi$ behavior, the linear component determined at low I values was subtracted and data were fitted for positive I values by the formula $I/I(2V) = (V/2)^\xi$. The charging energies were calculated by the formula given in the main text; all the experimental data necessary to calculate the charging energies are available in Table S1. Differences in absolute value of current at a finite voltage are hardly distinguishable (Fig. 4a and b). But the extraction of the power exponent ξ gives a good enough precision to statistically distinguish the current responses of the different systems (Table S1 and Fig. 4c).

Supplementary characterization data

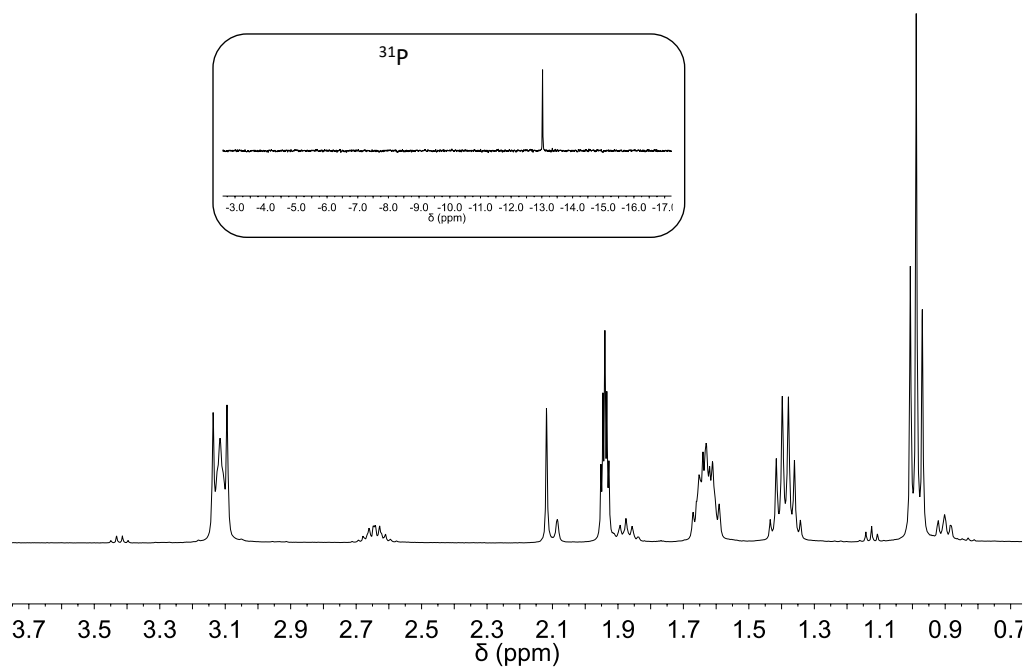


Figure S1. ¹H NMR (400 MHz) and ³¹P NMR (162 MHz, inset) spectra of **POM-P** in CD₃CN.

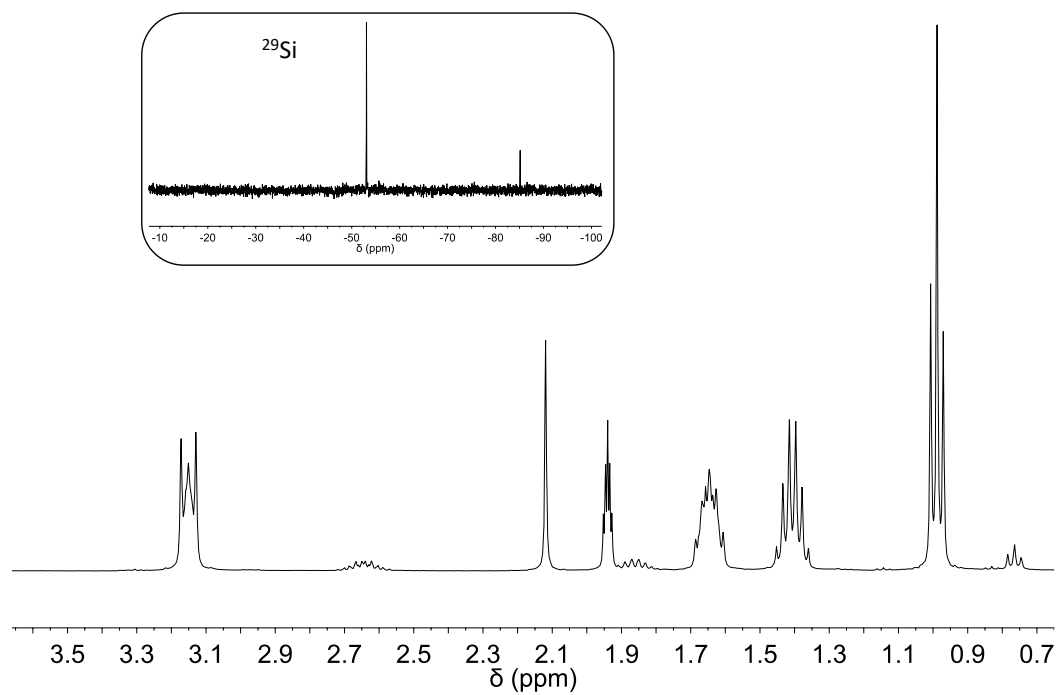


Figure S2. ¹H NMR (400 MHz) spectrum in CD₃CN and ²⁹Si NMR (119 MHz, inset) spectrum in DMSO-d₆ of **POM-Si**.

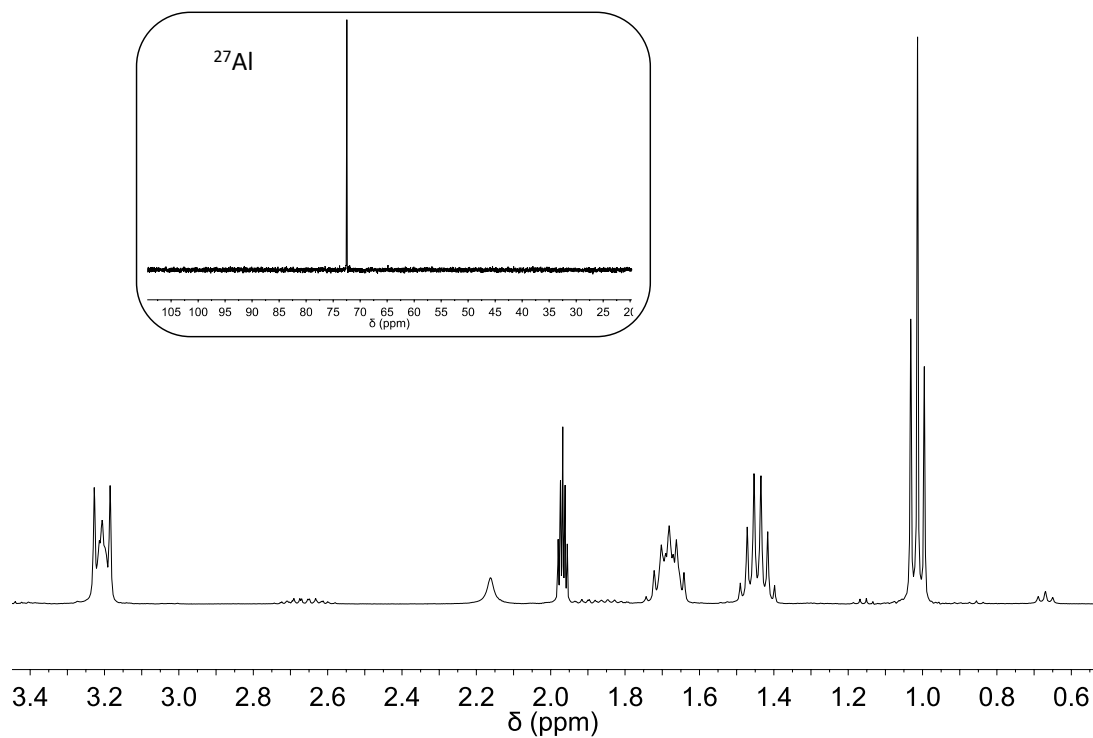


Figure S3. ^1H NMR (400 MHz) and ^{27}Al NMR (104 MHz, inset) spectra of **POM-Al** in CD_3CN .

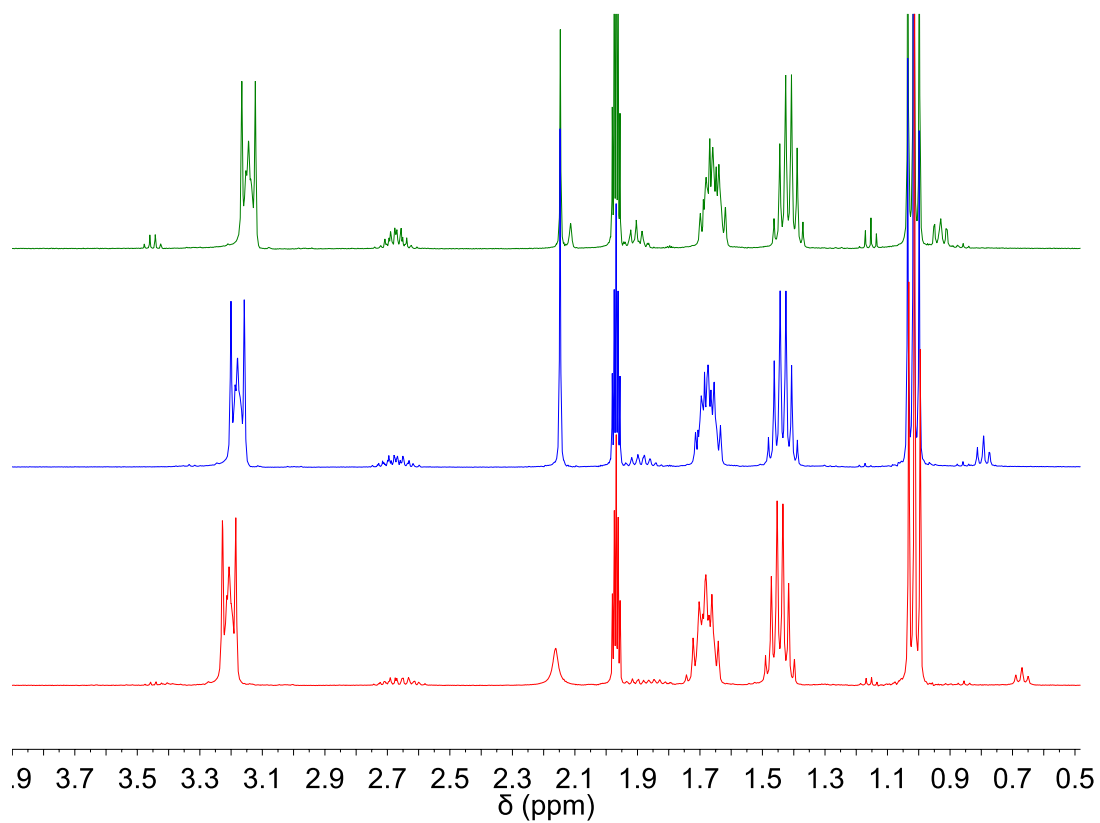


Figure S4. Stacking of the ^1H NMR spectra of **POM-P** (green), **POM-Si** (blue) and **POM-Al** (red).

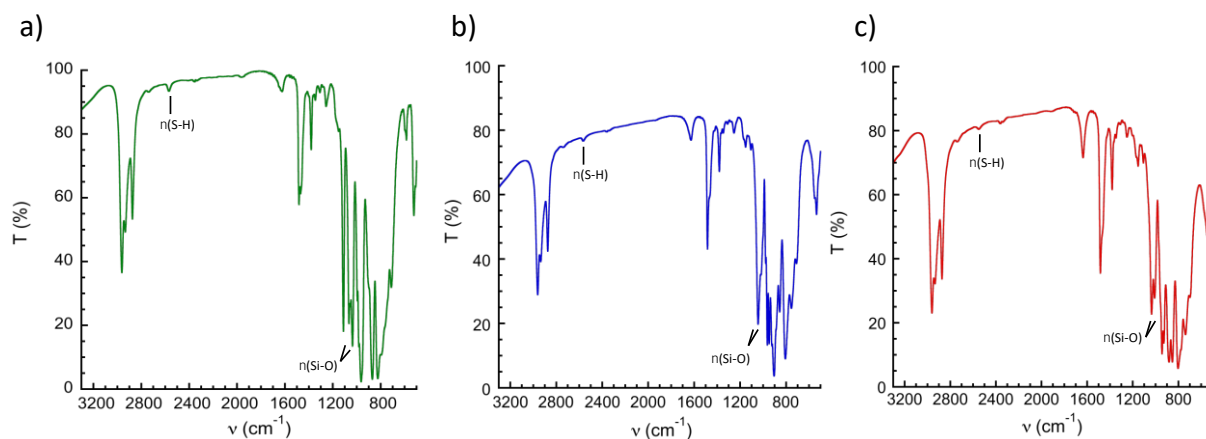


Figure S5. Infrared spectra from a KBr pellet of a) **POM-P**, b) **POM-Si**, c) **POM-AI**.

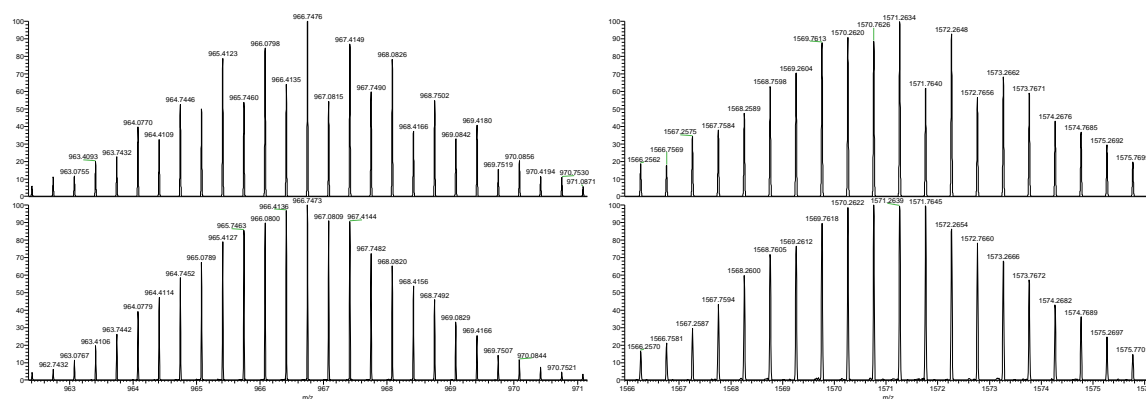


Figure S6. Comparison of calculated (upper trace) and experimental (lower trace) isotopic peaks for the ions $[C_6H_{14}O_{40}PS_2Si_2W_{11}]^{3-}$ (left) and $[C_{22}H_{50}NO_{40}PS_2Si_2W_{11}]^{2-}$ (right) of **POM-P**.

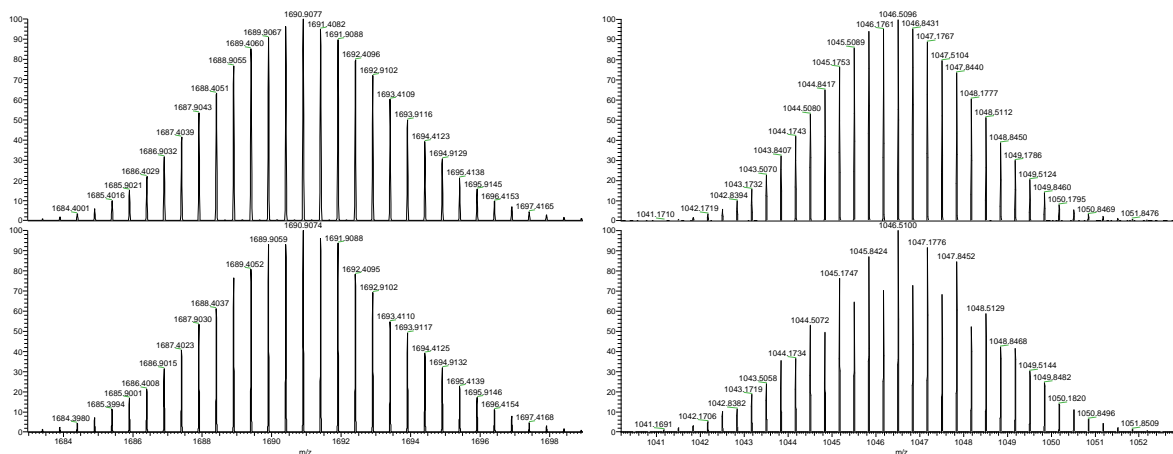


Figure S7. Comparison of experimental (upper trace) and calculated (lower trace) isotopic peaks for the ions $[C_{22}H_{50}NO_{40}S_2Si_3W_{11}]^{3-}$ (left) and $[C_{38}H_{86}N_2O_{40}S_2Si_3W_{11}]^{2-}$ (right) of **POM-Si**.

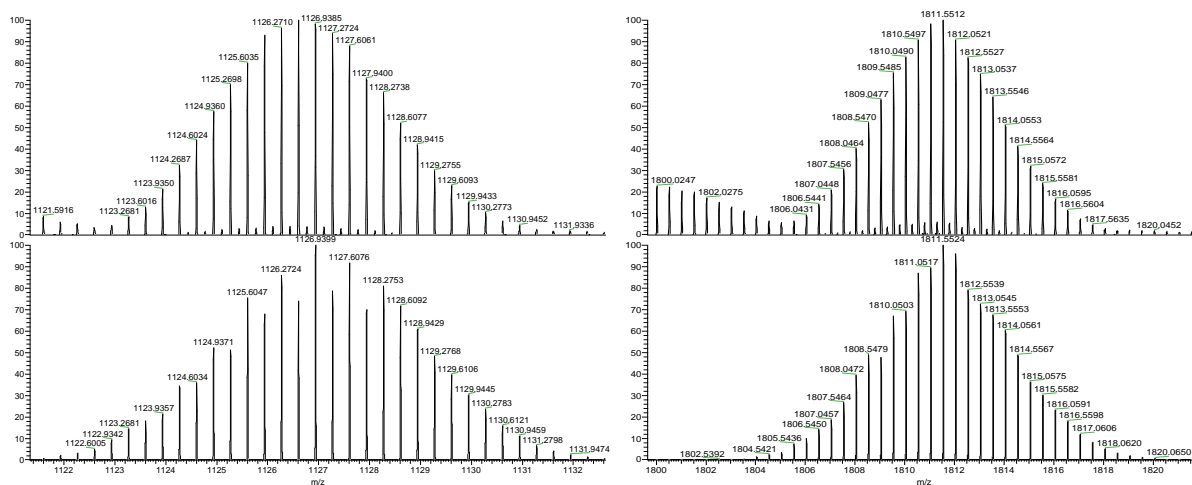


Figure S8. Comparison of experimental (upper trace) and calculated (lower trace) isotopic peaks for the ions $[C_{38}H_{86}N_2O_{40}AlS_2Si_2W_{11}]^{3-}$ (left) and $[C_{54}H_{122}N_3O_{40}AlS_2Si_2W_{11}]^{2-}$ (right) of **POM-Al**.

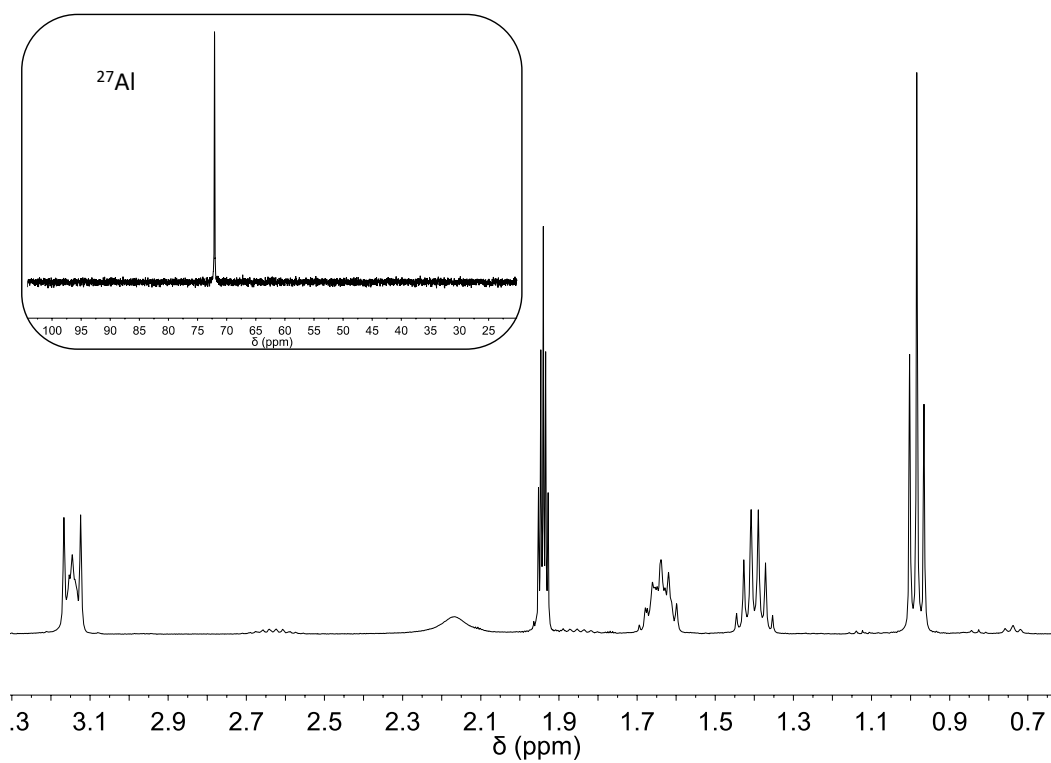


Figure S9. ^1H NMR (400 MHz) and ^{27}Al NMR (104 MHz, inset) spectra of **POM-AIH** in CD_3CN .

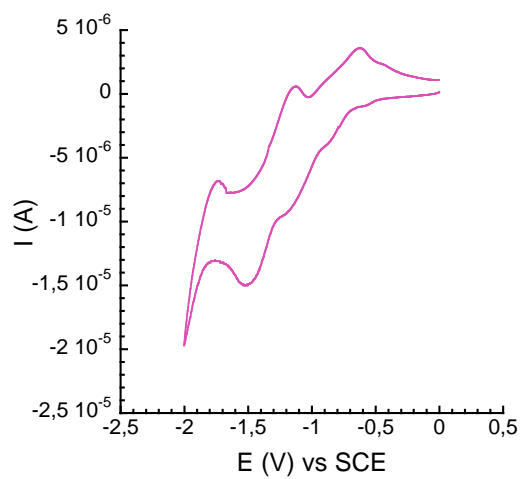


Figure S10. Cyclic voltammogram at a glassy carbon electrode of **POM-AIH** (1 mM) in a 0.1 M TBAPF_6 solution in CH_3CN at a scan rate of $0.1 \text{ V}\cdot\text{s}^{-1}$.

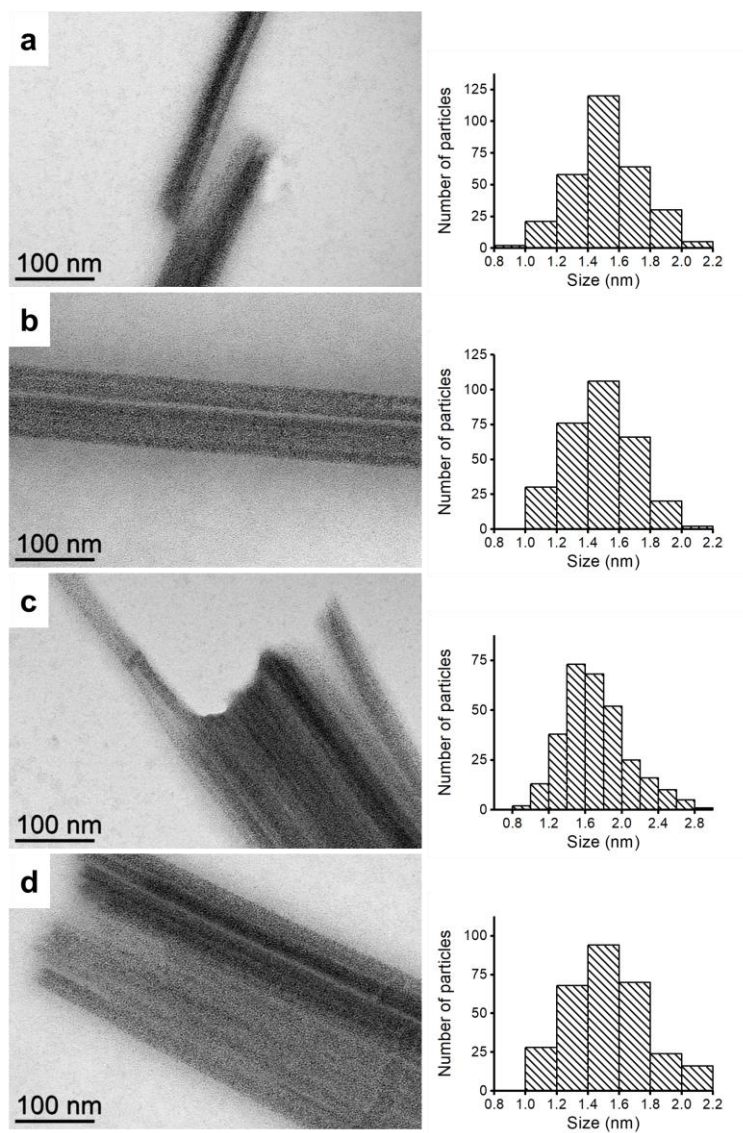


Figure S11. TEM pictures and size distributions of the Pt nanoparticles in the: a) **SA-AI** (1.5 ± 0.2 nm), b) **SA-Si** (1.5 ± 0.2 nm), c) **SA-P** (1.7 ± 0.4 nm), and d) **SA-AIH** (1.5 ± 0.2 nm) self-assemblies.

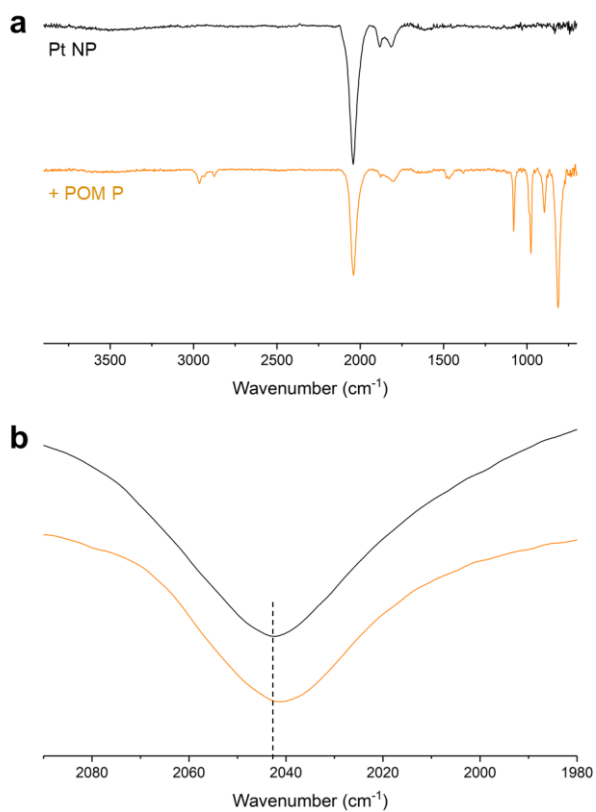


Figure S12. Infrared spectra of the pristine Pt nanoparticles and of a mixture of these Pt nanoparticles and unfunctionalized POM-P polyanions: a) full spectra and b) zoom on the terminal CO region (baselines are shifted for clarity – the dashed line is a guide for the eye); peak maxima: **Pt NP**: 2042 cm⁻¹, **Pt NP** + unfunctionalized **POM P**: 2041 cm⁻¹,

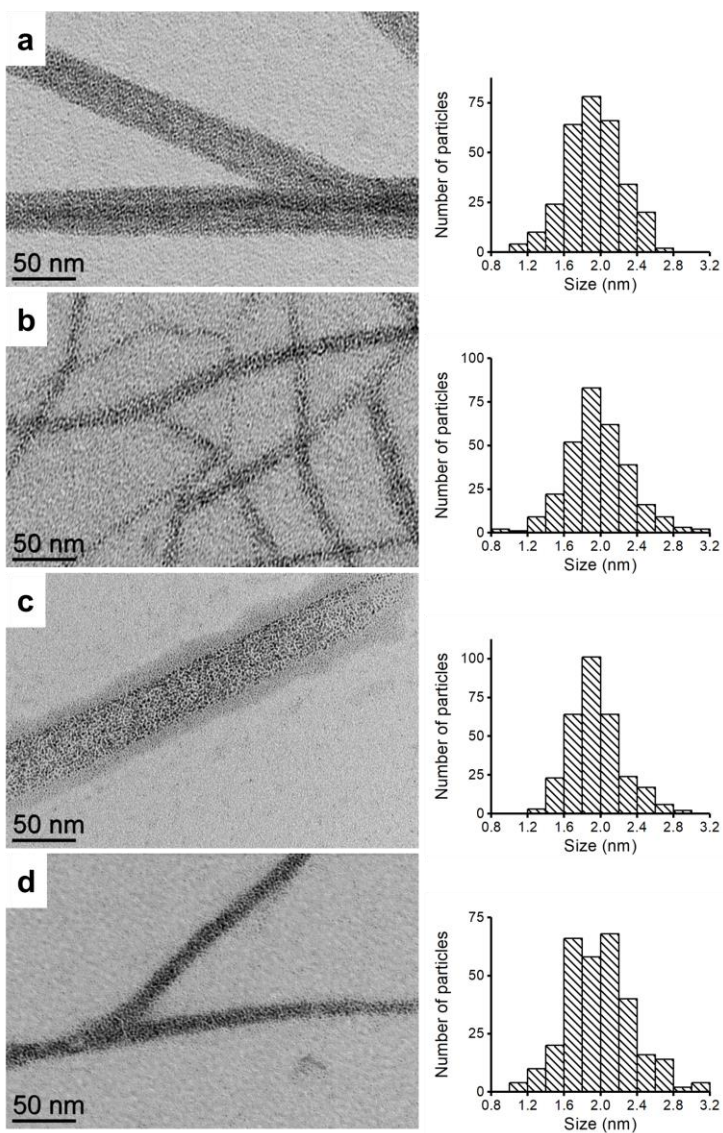


Figure S13. TEM pictures and size distributions of the Pt nanoparticles in the: a) **SA-Al-2** (1.9 ± 0.3 nm), b) **SA-Si-2** (2.0 ± 0.3 nm), c) **SA-P-2** (2.0 ± 0.3 nm), and d) **SA-AIH-2** (2.0 ± 0.4 nm) self-assemblies.

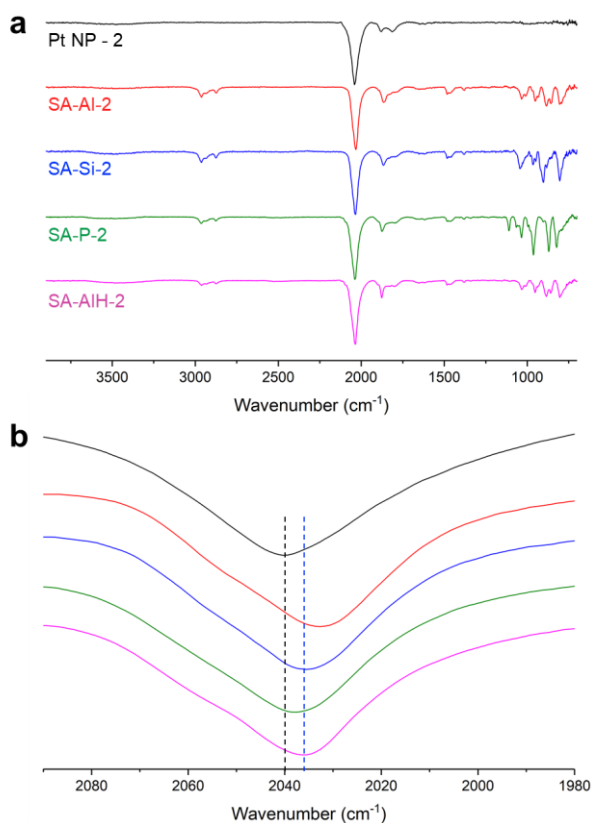


Figure S14. Infrared spectra of the pristine Pt nanoparticles and of the **SA-Al-2**, **SA-Si-2**, **SA-P-2**, and **SA-AIH-2** self-assemblies: a) full spectra and b) zoom on the terminal CO region (the baselines are shifted for clarity – the dashed lines are a guide for the eye); peak maxima: **Pt NP - 2**: 2040 cm^{-1} , **SA-Al-2**: 2032 cm^{-1} , **SA-Si-2**: 2035 cm^{-1} , **SA-P-2**: 2038 cm^{-1} , and **SA-AIH-2**: 2036 cm^{-1} .

	$d (\pm 0.05 \text{ nm})$	$s (\pm 0.05 \text{ nm})$	$\varepsilon_r (\pm 0.05)$	$E_c \text{ (eV)}$	ξ
SA-Al	1.5	2.4	3.10	0.63 ± 0.05	2.92 ± 0.06
SA-Si	1.5	2.4	3.36	0.58 ± 0.05	2.94 ± 0.07
SA-P	1.7	2.4	3.97	0.35 ± 0.03	2.19 ± 0.06
SA-AIH	1.5	2.4	3.51	0.56 ± 0.05	2.69 ± 0.06
SA-Al-2	1.9	2.8	3.10	0.43 ± 0.03	2.70 ± 0.07
SA-Si-2	2.0	2.8	3.36	0.34 ± 0.03	2.16 ± 0.06
SA-P-2	2.0	2.8	3.97	0.29 ± 0.02	1.94 ± 0.06
SA-AIH-2	2.0	2.8	3.51	0.33 ± 0.02	1.99 ± 0.07

Table S1. Nanoparticle size d , inter-particle distance s , dielectric constant of the POM ε_r , charging energy E_c , and power exponent ξ of the self-assemblies considered in the manuscript. d , s and ε_r are determined experimentally; E_c is calculated from these values with the equation given in the main text; and ξ is fitted from the I - V curves. Margins of error have been determined from the precision of measurements: trends of evolution for both E_c and ξ are significant (but a more precise study of differences falls within the margins of error).

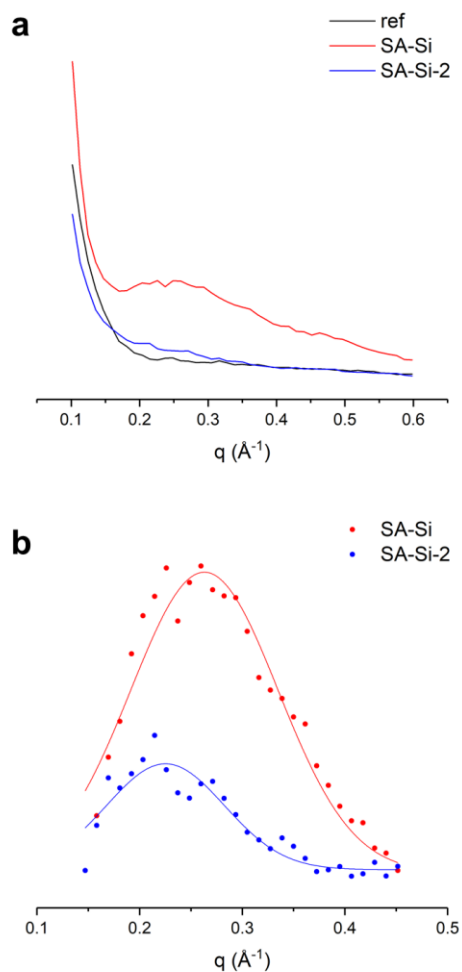


Figure S15. a) Small angle X-ray scattering patterns for the substrate alone (reference without any compound – ref) and for the **SA-Si** and **SA-Si-2** self-assemblies. The reference corresponds to the signal of the continuous background, whereas the self-assemblies show supplementary broad peaks, which corresponds to a specific correlation distance between the nanoparticles. b) SAXS patterns of the **SA-Si** and **SA-Si-2** self-assemblies after subtraction of the background signal and fit of the curves for estimation of the correlation distances ($s = 2\pi / q_{max}$): **SA-Si**: $q_{max} = 0.26 \text{ \AA}^{-1}$, $s = 2.4 \text{ nm}$; and **SA-Si-2**: $q_{max} = 0.22 \text{ \AA}^{-1}$, $s = 2.8 \text{ nm}$.